Discover Artificial Intelligence

Discover

Review

When medical images meet generative adversarial network: recent development and research opportunities

Xiang Li[1] · Yuchen Jiang[1] · Juan J. Rodriguez-Andina[2] · Hao Luo[1] · Shen Yin[3] · Okyay Kaynak[4]

Received: 8 June 2021 / Accepted: 12 July 2021
Published online: 22 September 2021

Abstract
Deep learning techniques have promoted the rise of artificial intelligence (AI) and performed well in computer vision. Medical image analysis is an important application of deep learning, which is expected to greatly reduce the workload of doctors, contributing to more sustainable health systems. However, most current AI methods for medical image analysis are based on supervised learning, which requires a lot of annotated data. The number of medical images available is usually small and the acquisition of medical image annotations is an expensive process. Generative adversarial network (GAN), an unsupervised method that has become very popular in recent years, can simulate the distribution of real data and reconstruct approximate real data. GAN opens some exciting new ways for medical image generation, expanding the number of medical images available for deep learning methods. Generated data can solve the problem of insufficient data or imbalanced data categories. Adversarial training is another contribution of GAN to medical imaging that has been applied to many tasks, such as classification, segmentation, or detection. This paper investigates the research status of GAN in medical images and analyzes several GAN methods commonly applied in this area. The study addresses GAN application for both medical image synthesis and adversarial learning for other medical image tasks. The open challenges and future research directions are also discussed.

1 Introduction

Deep learning has dominated the field of computer vision since 2012 [1], taking advantage of the huge improvement in data storage and computing power of modern processing devices. Currently, most advanced methods for computer vision are based on deep learning. In this context, medical image analysis is an important research direction. The advantage of deep learning network is the ability to automatically extract features [2], researchers can describe medical images without constructing complex manual features. In deep learning-based medical image analysis, the end-to-end network training method shows significant advantages. Moreover, medical image analysis has huge practical demand and market space. It can be reasonably predicted that deep learning-based medical image analysis has great potential for research in the near future.

Most current artificial intelligence (AI) methods and applications belong to the category of supervised learning [3], which in this case means medical image data must be labeled. This is very difficult and costly to achieve in practice. On one hand, each medical image implies in principle a patient behind it, so the amount of medical image data available

✉ Hao Luo, hao.luo@hit.edu.cn | [1]Department of Control Science and Engineering, Harbin Institute of Technology, Harbin 150001, China. [2]Department of Electronic Technology, University of Vigo, 36310 Vigo, Spain. [3]Department of Mechanical and Industrial Engineering, Faculty of Engineering, Norwegian University of Science and Technology, 7033 Trondheim, Norway. [4]Department of Electrical and Electronics Engineering, Bogazici University, Istanbul 34342, Turkey.

is very limited. On the other hand, medical image labeling requires highly specialized medical staff and plenty of time. For example, to train a deep convolutional neural network (CNN) for tumor segmentation, it is necessary for a specialized physician to mark all tumor pixels in the training image. These problems greatly restrict the development of automated, intelligent medical image analysis tools. It is of high potential that Generative adversarial network (GAN) has the potential to provide efficient solutions to these problems.

GAN was proposed in 2014 [4], with the original intention of imitating real data. GAN consists of two subnetworks: generator (G) and discriminator (D). During training, G is used to generate data with a given (expected) distribution, whereas D is used to determine whether generated data are real or fake. The two are trained alternately, and improve together [5]. Eventually, a G is obtained that can generate data close to the real data distribution, which is the ultimate goal of the method. Obviously, if it is applied to medical imaging, it can expand datasets with insufficient amounts of medical image data so that deep learning methods can be used together with the expanded datasets. Another very useful feature of GAN for medical image analysis is its adversarial training strategy, which can be applied to image segmentation, detection, or classification.

Compared with other medical image analysis techniques [6], GAN is still in its infancy and the number of related works available in the literature is relatively small, but it has huge potential. The application of GAN to medical images began in 2016, when only an article on the topic was published [7]. Since 2017, there have been more relevant studies, so the articles about GAN in medical images in the past five years have been analyzed and summarized in terms of application direction, methods, and other aspects. The rest of this article is organized as follows (Fig. 1). In the second section, GAN methods commonly applied in the medical image field are described in detail, focusing on their technical characteristics. The third section addresses the main application of GAN in this context, namely medical image synthesis. A classification is proposed according to different conditions of generation. The fourth section analyzes the application of GAN in medical image data enhancement. In the fifth section, GAN is discussed as a semi-supervised learning method, which mainly operates through feature and annotations sharing. The sixth section describes the functions of GAN that can be extended to other medical tasks. The seventh section discusses technical and non-technical challenges and directions. Finally, the conclusions are summarized in the eighth section.

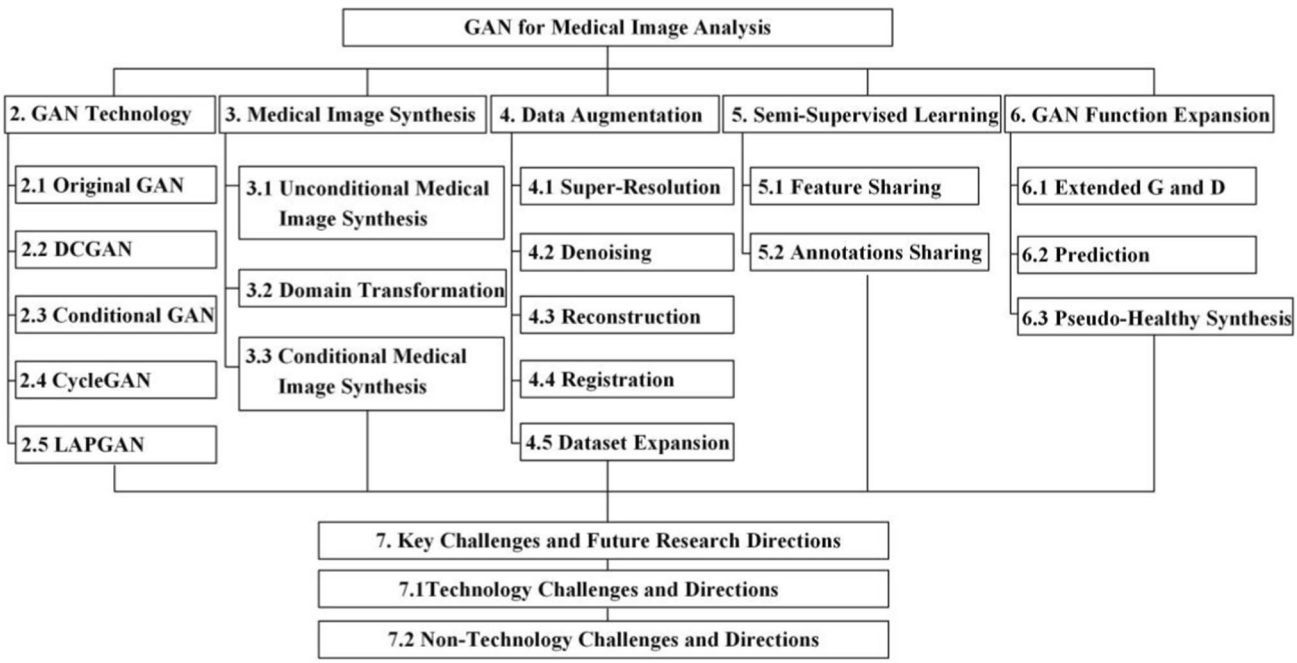

Fig. 1 Main content of this paper

2 GAN technology

This section starts with the original GAN and then covers the evolution process of GAN when used for image generation. The methods considered are also frequently used in the specific field of medical images. The section emphasizes the overall architecture, data flow, and objective function of GAN, and does not address the network details of specific generators or discriminators.

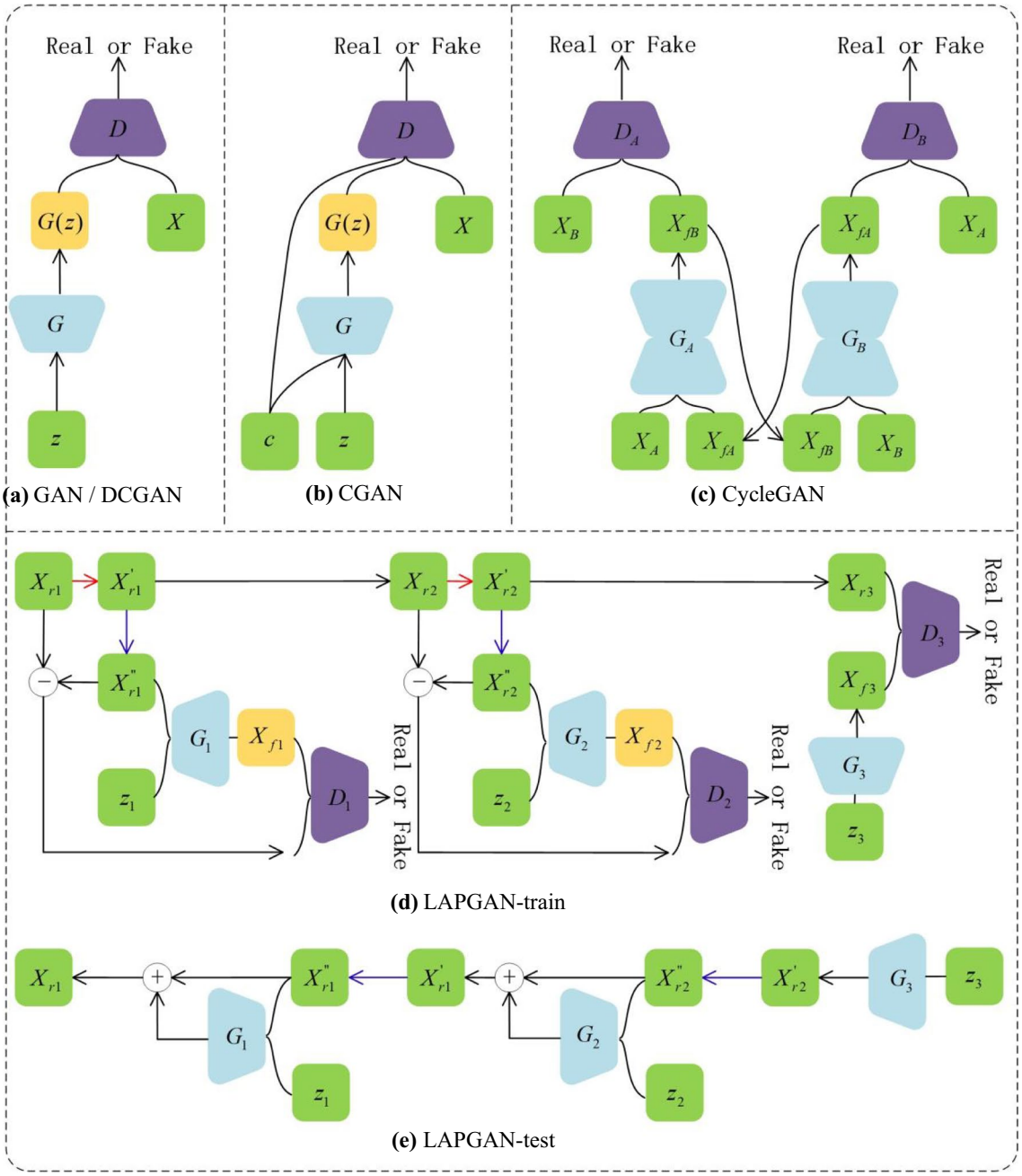

Fig. 2 Four common GAN structures

2.1 Original GAN

The operation of the original GAN is shown in Fig. 2a, where the symbols G and D denote neural networks. The input of G is a random noise vector z, which is sampled from the distributed $p(z)$. Generally, in order to keep consistency and convenience of training, the symbol $p(z)$ adopts either a Gaussian or a uniform distribution. It should be noted that z is a low-dimensional vector, whereas images in actual applications are high-dimensional data, so G learns the mapping from a low-dimensional noise space to a high-dimensional real data space. The inputs to D include $G(z)$, generated fake data, and X, real sample data used to balance training data. The symbol D is a classifier whose purpose is to judge the truth or falsehood of data. The purpose of G is to produce data as close to the real ones as possible, confusing D so that it cannot distinguish which ones are real and which ones are fake. In this way, G and D take part in a dynamic game process, improving each other during training. Data generated by G will be more and more realistic, and the recognition rate of D will gradually decrease from an initial value equal (or close) to 1 (perfect discrimination of real and false data) to (optimally) 0 (fake data cannot be distinguished from real ones). The optimization functions for D and G are as follows:

$$\begin{aligned} L_D &= \max_D E_{x\sim p(x)}\left[\log D(x)\right] + E_{z\sim p(z)}\left[\log(1 - D(G(z)))\right], \\ L_G &= \min_G E_{z\sim p(z)}\left[\log(1 - D(G(z)))\right] \end{aligned} \tag{1}$$

where L_D and L_G represent D and G loss functions, respectively, $D(x)$ is close to 1, because X are real data,$D(G(z))$ gradually decreases, and the optimization process consist in maximizing L_D and minimizing $\mathrm{L_G}$.

2.2 DCGAN

The original GAN is not actually used to generate images, because G and D are ordinary fully connected networks not suitable for images. Image data distribution is very complex and has high dimensions, which is not easy to achieve. CNNs are more image-friendly than fully connected networks, and deep convolutional generative adversarial networks (DCGAN) have successfully combined CNNs with GAN, resulting in a more suitable solution for image generation [8]. DCGAN also adopts the structure shown in Fig. 2a, except that G and D are both replaced by CNNs. GAN has the problem of mode collapse, in other words, the training process is not stable, and generated images may only belong to a few fixed categories, or some strange images may appear. DCGAN proposes a series of techniques to balance the training process. G and D are fully convolutional networks (FCNs, i.e., CNNs without fully connected layers), using strided convolution instead of pooling layer for down-sampling. The output layer of G and the input layer of D use batch normalization [9], a data normalization layer that can be embedded in the network to accelerate learning and convergence. In DCGAN, activation functions are also changed in D with regard to GAN. GAN uses the ReLU activation function [10] (Fig. 3a) for both G and D, whereas DCGAN uses ReLU for G and LeakyReLU [11] (Fig. 3b) for D, to prevent gradient sparsity. In addition, the activation function of the output layer of D is tanh.

2.3 CGAN

GAN uses a random noise vector with a very low dimension to generate high-dimensional image data. This modeling method has too many degrees of freedom. If the noise signal has only hundreds of dimensions but the generated image

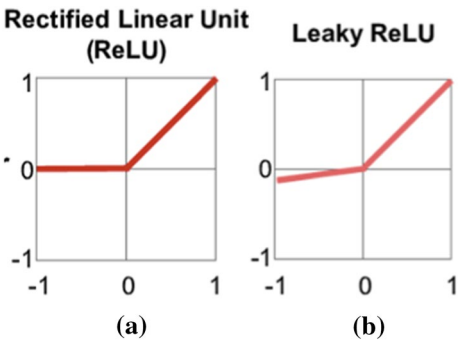

Fig. 3 ReLU and Leaky ReLU activation functions

has thousands of pixels, then controllability will be very poor. Conditional generative adversarial networks (CGAN, Fig. 2b) increase controllability by adding a constraint c to data [12], which is part of the input layer of both G and D, guiding data generation. The objective function of CGAN is

$$\begin{aligned} L_D &= \max_D E_{x\sim p(x)}\left[\log D(x|c)\right] + E_{z\sim p(z)}\left[\log(1 - D(G(z|c)))\right], \\ L_G &= \min_G E_{z\sim p(z)}\left[\log(1 - D(G(z|c)))\right] \end{aligned} \tag{2}$$

where c can be a label, tags, data from different modes, or even an image. For example, the prior condition (see Sect. 3.3) used by Pix2pix [13] is segmentation image or contour image, Pix2pix can complete the transformation from image to image. When the prior condition is an image, a loss between conditional and generated images is usually added, so that the generated image can have higher authenticity [13]. InfoGAN [14] can also be viewed as a special kind of CGAN. Different from CGAN, it tries to add constraints in random noise z and uses regularization terms based on mutual information. As the input of the network, the symbol z controls the image generation. For instance, in the MNIST dataset [15], z controls the thickness, slope, and other characteristics of the generated numbers.

2.4 CycleGAN

Pix2pix requires paired images, one of them annotated, which requires a lot of time and implies a high cost. In contrast, CycleGAN [16] proposes a ring closed network consisting of two generators and two discriminators (Fig. 2c), which performs the conversion between two image domains without the need of paired images. Because of the two generators and discriminators, the overall structure and data flow are more complex than in the previous methods. The symbols G_B and G_A perform the transformation from domain A to domain B and from domain B to domain A, respectively, so they are equivalent to two reciprocal mappings. The symbol G_B generates images X_{fB} with domain B characteristics from images X_A of domain A, whereas G_A generates images X_{fA} with domain A characteristics from images X_B of domain B. Discriminators D_A and D_B identify images of domains A and B, respectively. The objective function of CycleGAN can be written as:

$$\begin{aligned} L(G_A, G_B, D_A, D_B) &= L_{GAN}(G_A, G_B, X_A, X_B) \\ &+ L_{GAN}(G_B, G_A, X_B, X_A) + \lambda L_{cyc}(G_A, G_B) \end{aligned} \tag{3}$$

where L_{GAN} is a regular generator loss, as described by Eq. (1). Real data return to its original domain after a loop, so L_{cyc} represents the loss of real data and its cyclic data. λ is a coefficient used to balance generator loss and cycle loss.

$$\begin{aligned} L_{cyc}(G_A, G_B) &= \mathrm{E}_{X_A\sim A}\left[\left\|G_A(G_B(X_A)) - X_A\right\|_1\right] \\ &+ \mathrm{E}_{X_B\sim B}\left[\left\|G_B(G_A(X_B)) - X_B\right\|_1\right] \end{aligned} \tag{4}$$

Since it is easy for GAN to be unbalanced in training, the two generators and discriminators in CycleGAN need to be carefully balanced during training. The use of paired images is equivalent to a feature filtering, and GAN can easily learn which parts of images need to be converted. However, the training process requires huge amounts of data when working with unpaired images, like in the case of CycleGAN.

2.5 LAPGAN

Humans usually paint a picture with multiple strokes, so machines can create images by multiple steps. That is where the idea of LAPGAN [17] comes from. There is no need to complete all GAN tasks at once, but one at a time generating a full image in several steps. Figure 2d shows a three-stage LAPGAN, the red arrows representing down-sampling and the blue arrows representing up-sampling. The three down-sampling processes can be regarded as a three-layer Laplace pyramid, and an independent conditional GAN model is trained at each level. Using the multi-scale structure of natural images, a series of generative models are constructed, each one capturing a specific scale image structure of the pyramid. The training process is carried out from left to right. The original image X_{r1} is transformed into X'_{r1} through down-sampling, and X'_{r1} becomes X''_{r1} through up-sampling. Then a residual image is obtained by comparing X_{r1} with X''_{r1}. G_1 takes a noise signal z_1 as input and X''_{r1} as the condition to generate the residual image. Training in the remaining levels is similar. The LAPGAN test process is shown in Fig. 2e. In this case it is performed from right to left. It is important

to note that the target of G is the residual image, so there is a summation process. Serialization and the use of residual images are the two LAPGAN characteristics that effectively reduce the content and difficulty that GAN needs to learn.

3 Medical image synthesis

The most successful application of GAN in medical image analysis to date is medical image synthesis, which can alleviate the problems of insufficient medical images available or imbalanced data categories [18, 19]. Traditional data enhancement techniques include image cutting, flipping, and symmetry, among others. Obviously, these techniques can only change data in direction or size, but no new data are generated, whereas GAN can generate completely new data. In this section, unconditional synthesis, domain transformation and other conditional synthesis methods are described according to different conditions of medical images. Figure 4 shows some examples of these applications.

3.1 Unconditional medical image synthesis

Unconditional synthesis was the first method used in medical image analysis. It is usually a tentative method in preliminary studies or when constraints are not available. A random noise is transformed into an image. Since the information contained in random noise is very small compared with that of a large image, the resolution of generated images is usually not very high. DCGAN and LAPGAN are the most commonly used methods for unconditional medical image synthesis.

Medical images of the brain, chest, organs, and fundus are usually taken at very high resolution, so synthesized images must have reasonable outline, shape, and structure to look realistic enough. Therefore, it is in principle difficult to use unconditional synthesis to generate such complex images. Camilo et al. [20]. proved that unconditional synthesis could generate high-resolution images. They used one-dimensional uniform noise as input to G, and generated brain MRI images with a resolution of 220×172. In [27], Wasserstein GAN (WGAN) was used to generate 128×128 brain MRI slices. Furthermore, for synthesis of brain MRI slices, in [28] a Laplace pyramid adversarial network was designed and

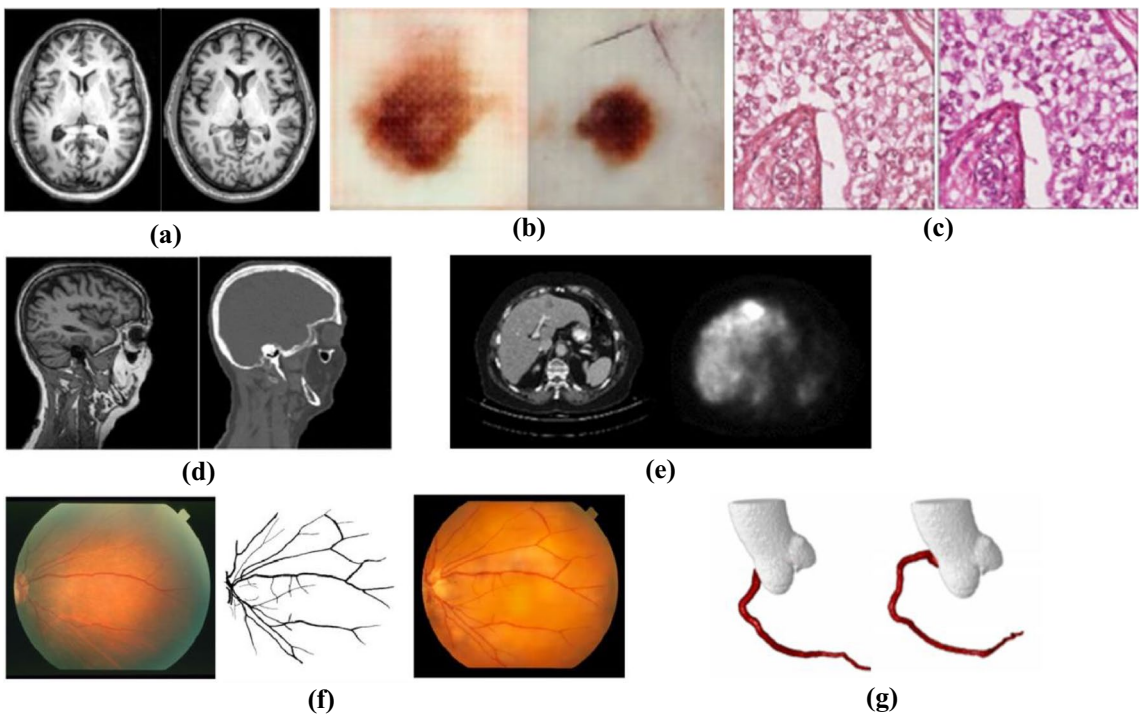

Fig. 4 Medical image synthesis examples. Unconditional synthesis of brain magnetic resonant images (MRI) [20] **a** and of skin lesions [21] **b** synthesized (left) and real (right) images. **c** Stain normalization by GAN [22]: original (left) and stained (right) images. **d** MRI image (left) converted into computed tomography (CT) image (right) [23]. **e** MRI image (left) converted into positron emission tomography (PET) image (right) [24]. **f** Retinal vessels used as condition to generate color fundus image [25]: original color fundus image (left), retinal vessels map (center), synthesized color fundus image (right). **h** Blood vessel geometry synthesis [26]

implemented by building a series of generative models, each one capturing a specific image structure. A low-resolution image is first generated, and then more details are gradually added to it to generate the high-resolution image. Progressively grown generative adversarial networks (PGGAN) have also been applied in [21], where colored fundus images from 8 to 512 pixels were synthesized. In order to balance the amount of data in different categories, Hojjat et al. [29] proposed to use DCGAN. They generated six different categories of chest X-ray (CXR) images.

In contrast with the generation of medical images that contain a whole structure, many researchers targeted lesion sites, such as tumors or plaques, which are usually smaller in size and easier to be synthesized. Andy and Jarrel [30] used GAN to synthesize images of prostate lesions with 16×16 resolution. In [31], images of benign and malignant pulmonary nodules were generated with a resolution of 56×56 and image fidelity even fooled expert doctors. Christoph et al. [32, 33] used DCGAN and LAPGAN to generate images of skin lesions, results showing that LAPGAN was more effective. Xin et al. [34] proposed catWGAN, where categorical generative adversarial networks (catGAN) was the primary structure and WGAN the auxiliary network, to generate images of cutaneous melanoma tissue. Maayan et al. [35] synthesized high-quality liver damage ROIs using GAN structures, then a hepatopathy classification network was trained using traditional enhanced data and synthetic data, results showing that synthetic images are completely competent for classification. Table 1 summarizes published methods for unconditional medical image synthesis. Since unconditional medical image synthesis mostly takes random noise vectors as input, only model output is given in Table 1. Measures refer to the method used to evaluate the how realistic the synthetic images are.

3.2 Domain transformation

Domain transformation is one of several existing conditional synthesis methods but, because of the many published works that use it and also because it is a special condition, it is described separately in this subsection.

Domain transformation refers to the transformation from one type of image into another. MRI and CT are the most widely used medical images, and domain transformations between them account for nearly half of all domain transformation published works. MRI is better than CT in terms of imaging, but requires the patient to lie still for a long time, and he/she cannot have metal in the body, so some patients are only suitable for CT. On the other hand, CT can expose patients to risk of cancer, so some patients are only suitable for MRI. In this context, domain transformation helps doctors make a comprehensive judgment of patients who can only take one kind of image.

Dong et al. [36] proposed a FCN as generator to transform brain MRI images into CT ones by adopting the strategy of adversarial training. The input of the FCN is the MRI image, and the label is the corresponding CT image. Since images are in the form of patches, auto-context model is also used to construct context information. Differently, [23] used unpaired data, meaning that the MRI and CT images were not from the same patient at the same location, and CycleGAN was used to carry out the conversion between unpaired images. Zhao et al. [37] designed a kind of depth supervision cascade

Table 1 Summary of publications for unconditional medical image synthesis

Method	Dataset	Output	Anatomic site	Measures	Resolution
[20] DCGAN	BLSA	T1-MRI	Brain	Expert assessment	220×172
[27] DCGAN WGAN	BRATS2016	Multi-modality MRI	Brain	Expert assessment	128×128 64×64
[28] GAN	Private dataset	T1-MRI	Brain	Kernel Density function Expert assessment	128×64
[21] PGGAN	i-ROP BRATS2017	Retinal fundus images Glioma multi-modality MRI	Eye Glioma	Based on data distribution	512×512 256×256
[29] DCGAN	Private dataset	X-rays	Chest	Expert assessment	256×256
[30] DCGAN	SPIE ProstateX Challenge 2016	multi-modality MRI	Prostate	None	16×16
[31] DCGAN	LIDC-IDRI	CT	Lung Cancer	Expert assessment	56×56
[32] DDGAN	ISIC2017	skin lesions	Skin Lesions	Wasserstein Distances	256×256
[33] PGAN	ISIC2018	skin lesions	Skin Lesions	Expert assessment	256×256
[34] catWGAN	ISIC2016 PH2	skin lesions	Skin Lesions	Based on data distribution	128×128
[35] DCGAN	Private dataset	CT	Focal Liver Lesions	Expert assessment	64×64

GAN, which they applied for automatic segmentation of bone structures. The first module in the network is used to generate high quality CT images from MRI ones, and the second module is used to segment bones from the generated CT images. In [38], a 3D generation network based on CycleGAN was proposed, which transformed 3D cardiovascular volume MRI images into CT images, adding a loss function for shape. The generated image is segmented to measure the gap between generated and real data. Thomas et al. [39] also used unpaired cardiac MRI and CT images. Yuta et al. [40] proposed gradient consistency loss for CycleGAN to place more emphasis on the boundary between joints and muscles, so the resulting images have clearer boundaries.

PET has also been the subject of many works on image domain transformation. Avi et al. [24] used a VGG16 CNN as generator to transform CT images into PET ones, with very small datasets consisting of only 17 pairs of training samples and 8 pairs of test samples. Lei et al. [41] aimed at low resolution and low signal-to-noise ratio synthetic PET images. They proposed a multi-channel GAN, which can capture features with advanced semantic information based on the concept of dual learning. This method produces PET lung cancer images are very close to real ones. In [42] a sketcher-refiner GAN composed of two CGAN is proposed to predict the content of pet-derived myelin in multimodal MRI. Karim et al. [43] proposed a new GAN framework (MedGAN) and a new generator (CasNet) for converting PET images into CT ones. MedGAN captures high- and low-frequency components of the target mode through a new combination of adversarial framework and non-adversarial losses. CasNet is inspired by residual neural networks (ResNets), where several fully convolutional encoder-decoder networks are connected together as generator. In [44], an FCN is used to transform CT images into initial PET images, which are then improved and refined with CGAN.

Other interesting application of medical image domain transformation is microscopic examination of human tissue, which requires chemical staining to produce contrast. Similar tissues may differ greatly in appearance depending on the stain, scanner, slice thickness, and experimental environment. This randomness of stain poses a great challenge to the automatic analysis of medical images. It is possible for GAN to achieve automatic stain generation or to transform different staining images into the same style. Aicha and Ghassan [22] proposed a stain normalization method and designed a discriminating image analysis model with a stain normalization component. It can learn the dyeing properties of a particular dataset, different types of images can be normalized, and then other image tasks can be performed (e.g., classification or segmentation). Farhad et al. [45] tested three stain normalization methods, namely GAN, variational auto-encoder (VAE), and deep convolutional Gaussian mixture model (DCGMM), among which DCGMM provided the best results. In [46], the first two components of principal component analysis (PCA) and the average image built a three-channel color image as the condition, then CGAN was used to complete the stain of lung histology images. Published methods for medical image domain transformation are summarized in Table 2. Table 2 also shows the evaluation metrics of synthetic images, the commonly used metrics include synthetics Mean Squared Error (MSE), Structural Similarity Index (SSIM), and Peak Signal to Noise Ratio (PSNR). Visual Information Fidelity (VIF), Universal Quality Index (UQI), and Learned Perceptual Image Patch Similarity (LPIPS) are also adopted in few works.

3.3 Conditional medical image synthesis

Several different prior conditions can be used in conditional medical image synthesis. In addition to domain transformation, segmentation map is the most commonly used prior condition among the many existing ones. In it, the segmentation task consists in obtaining the segmentation map from the original image, and the generation task consists in regenerating from the segmentation map the original image, whose style may change in the process. Therefore, these can be regarded as inverse tasks to each other.

He et al. [25] proposed a GAN that can synthesize color fundus images based on retinal vessel maps and designed a style extractor based on VGG16. The features of the style extractor middle layer were added to GAN in the form of style loss. Retinal vessel maps are the input of GAN, and any style color fundus image can be used as the input of the feature extractor, which converts vessel maps into color fundus images. This method produces a variety of color fundus images, but the retinal vessels are fixed. In [47], VAE is used to reconstruct retinal vessels and then to generate color images. In [48], two GAN are used, one to generate retinal vessels from random noise, and then another to generate color fundus images. Hu et al. [49] used the calibrated pixel coordinates of global physical space as a prior condition to generate fetal ultrasound images. Francis and Debdoot [50] used the speckle mapping of a digitally defined phantom as condition, and then pathological ultrasound images were generated after two-stage GAN. In [51], the generating condition is set as real image. GAN's role is to add different disease features into healthy images to generate realistic CXR images with different diseases. Lejmer et al. [26] used an attribute vector containing real sample and synthetic sample information as condition, then synthesized 3D coronary geometry figures with CGAN. Magnetic resonance angiography (MRA) is

Table 2 Summary of publications for medical image domain transformation

Method	Dataset	Input	Output	Anatomic site	Measures	Resolution
[36] GAN Auto-Context	ADNI Private dataset	MRI	CT	Brain Pelvic	MAE PSNR	32×32×32 153×193×50
[23] CycleGAN	non-public	MRI	CT	Brain	MAE PSNR	183×250×250 183×259×259
[37] U-net VGG	ADNI	MRI	CT	Cranium	Downstream tasks	152×184×5
[38] CycleGAN	Private dataset	MRI CT	CT MRI	Cardiovascular	Shape quality Dice score	86×112×112 86×112×112
[39] CycleGAN U-net	Private dataset	CT	MRI	Cardiovascular	Dice score	232×232×10 232×232×5
[40] CycleGAN	Private dataset	MRI	CT	Muscles	MAE PSNR	256×256×38 256×256
[24] CGAN FCN	Private dataset	CT	PET	Liver	True Positive Rate False Positive Rate	70×70
[41] M-GAN	Private dataset	CT	PET	Lung	MAE PSNR	512×512 200×200
[42] Sketcher-Refiner GAN U-net	Private dataset	MRI	PET	Brain	Mean DVR values	None
[43] MedGAN CasNet	Private dataset	PET	CT	Brain	SSIM PSNR MSE VIF UQI LPIPS	400×400 512×512
[22] DCGAN	ICPR'14 MICCAI'16 Private dataset	Histopathology image	Normalized image	Breast Colon Ovarian	Downstream tasks	250×250
[45] GAN VAE DCGMM	Private dataset	Histopathology image	Normalized image	Lymph nodes	Standard Deviation Coefficient of Variation	299×299 576×576
[46] Spectral Radiance Calibration PCA CGAN	Private dataset	Histopathology image	Normalized Image	Lung	SSIM MSE	64×64

Table 3 Summary of publications for conditional medical image synthesis

Method	Dataset	Condition	Output	Anatomic site	Measures	Resolution
[25] CGAN VGG	DRIVE STARE HRF NeuB1	Vessel image	Fundus image Neuronal image	Eye Neuro	Downstream tasks	512×512
[47] VAE-GAN	DRIVE	Vessel image	Retinal image	Vessel	ISC	565×584
[48] CGAN DCGAN	DRIVE	Vessel image	Retinal image	Vessel	Downstream tasks	512×512
[49] Spatially-conditioned generative adversarial learning	SPACE FANST	Anatomical landmark	Ultrasound image	Fetal profile	Acc 2D distances	160×120
[51] CGAN	SCR	X-ray image	Chest images	Lung	Downstream tasks	512×512
[26] CGAN	Private dataset	Vector containing sample information	Coronary geometry	Artery	None	None
[52] Baseline GAN sGAN	IXI	T1 and T2 MRI images	2D MRA axial slices	Brain	PSNR Dice	512×512×100

an important imaging technique, usually captured for vascular intervention, but the MRA sequence may be missing in patient scans. Sahin et al. [52] proposed a MRA generation method based on T1-weighted and T2-weighted MRI images. Published methods for conditional medical image synthesis are summarized in Table 3.

4 Data augmentation

Although there has been a lot of work for medical image synthesis, the ultimate purpose of GAN application in the field of medical imaging is to improve the performance of the models, such as classification or segmentation models. Small dataset size and poor image quality reduce the accuracy of deep learning medical image models. To overcome these problems, some researchers use GAN technology for data augmentation, including super-resolution, image denoising, reconstruction, registration, and dataset expansion. In fact, image synthesis can also be regarded as a kind of data augmentation, but there is a lot of work on medical image synthesis, we use a separate chapter to introduce image synthesis.

4.1 Super-resolution

Super-resolution technology refers to the generation of high-resolution images from low-resolution ones, to obtain more detailed information. The super-resolution of medical images using GAN technology mainly relies on the capabilities of the generator. GAN-based medical image super-resolution is usually based on pairs of low- and high-resolution images. Almalioglu et al. [53] proposed a framework combining an attention mechanism with CGAN and designed a high-fidelity loss function. This is a weighted hybrid loss function specifically optimized for endoscope images, which synergistically combines the benefits of perception, content, texture, and pixel-based loss description. Ma et al. [54] proposed a GAN-based progressive multi-supervised super-resolution model, whose first stage corresponds to a densely-connected U-Net CNN [55], whereas the generator of the second stage corresponds to a residual-in-residual DenseBlock CNN.

In the field of medical imaging, high-resolution images require better equipment or longer image processing, and the acquisition of paired low- and high-resolution images is difficult. For example, to obtain paired high and low-resolution CT images, patients are required to undergo multiple CT scans with additional radiation dose, which is obviously not feasible. Therefore, some researchers use unsupervised or semi-supervised GAN methods for super-resolution. Daniele et al. [56] used the cyclic consistency method for microscopic endoscopic images. They designed a deep learning framework for unsupervised training with two special loss functions, in which paired low- and high-resolution images are no longer required. GAN's function is to convert a low-resolution image in the input domain into an image in any target domain. You et al. [57] incorporated residual learning into network technology for feature extraction and recovery. They also enforced cyclic consistency according to the Wasserstein distance, and included joint constraints in the loss function to achieve structural protection. Das et al. [58] use adversarial learning with cycle consistency and identity mapping prior conditions to preserve spatial correlation, color, and texture details in generated clean HR images. As it can be seen, most existing unsupervised super-resolution methods are based on cyclic consistency loss.

Deep CNNs require a large number of parameters to be optimized and a large amount of memory to be used. The problems discussed above are all focused on 2D images. When reconstruction takes place in a 3D environment, processing times for both training and inference need to be considered [59]. Chen et al. [60] proposed a multistage dense connection network with GAN for 3D brain MRI super-resolution reconstruction. The generator convolutional layers are all connected in a dense manner, whose main advantage is high speed. Irina et al. [61] used a combination of least squares dual loss and image gradient as loss function for the generator in GAN 3D super-resolution reconstruction, improving the quality of generated images.

4.2 Denoising

Noise in medical images seriously affects the diagnostic accuracy of doctors. This problem can be alleviated by GAN image denoising capabilities. In CT images, since high doses can harm the patient's health, the past decade has seen a trend towards dose reduction in CT examinations, at the expense of noise appearing in the low-dose images. Yang et al. [62] proposed a GAN with Wasserstein distance and perceptual similarity, which suppresses noise by comparing the perceptual features of a denoised output against those of the ground truth in a given feature space. Wolterink et al. [63] compared three training strategies, namely voxel loss, combined voxelwise and adversarial loss, and adversarial loss.

Choi et al. [64] considered the statistical characteristics of CT images and introduced a loss function to incorporate the noise property in the image domain derived from noise statistics in the sinogram domain.

In addition to the use of lower doses, operation equipment (e.g., portable) may also introduce noise. Zhou et al. [65] constructed a two-stage GAN to improve the quality of ultrasonic images and reduce noise. In the training process, a transmission learning method based on plane wave image (PWI) data was introduced to facilitate convergence and eliminate the influence of deformation caused by respiratory activity. Chen et al. [66] proposed an unsupervised learning framework for high-quality pixel-level smoke detection and removal. The detection network is regarded as a prior knowledge and a loss function is used to support the training of smoke removal network.

4.3 Reconstruction

MRI is a widely used clinical medical imaging method, but one of its main disadvantages is the long acquisition time. During MRI imaging, data samples are not collected directly in the image space, but in the k space. The k space contains spatial frequency information obtained row by row and at any position. Slow acquisition causes interferences that may reduce image quality, due for instance to patient movements, such as heart beats or breathing. Compressive sensor-based imaging provides a solution to accelerate the acquisition of MRI images by reconstructing them from a small part of k space. In theory, assuming that the original data can be compressed, the reconstruction can be performed through nonlinear optimization of random under-sampled original data. GAN-based MRI image reconstruction is based on this theory and can be summarized as follows. The generator consists of multiple end-to-end networks. The first one converts a zero-fill reconstructed image into a complete reconstructed image. The following refinement network improves the accuracy of the reconstructed image. Then a discriminator network assesses whether or not the reconstruction is accurate. The works reported in [67, 68, 69] are all based on this framework, whose structure is shown in Fig. 4, the difference being the loss functions used. In order to improve the perceived quality of reconstruction [67], content loss is designed for generator training. This loss includes three parts: pixel mean square error loss, frequency domain mean squared error loss, and VGG loss. Feature matching loss and penalty are added in [68]. The work in [69] adds cycle loss, which is a cycle combination of low sampling frequency and completely reconstructed images.

4.4 Registration

To get accurate pathological information in the process of medical diagnosis, a set of images is taken of the same body part, so it is usually necessary to conduct quantitative analyses of several different images at the same time. These images need to be strictly aligned, which is called image registration. It requires a spatial transformation of images, so that there is spatial consistency between corresponding points in several images. In [70], a constrained CNN replaced heuristic smoothness measures of displacement fields, the generator is the registration network and the discriminator distinguishes the dense displacement field predicted by the generator from motion data simulated with the finite element method. During training, the registration network maximizes the similarity between anatomical labels and minimizes the difference between measured and simulated deformation. The generator in [71] generates conversion parameters between fixed and moving images. Different from [70], the discriminator is not used to assess conversion parameters, but to determine whether or not the processed moving image has completed registration. The work in [72] used CGAN for multimodal registration. By adding appropriate terms into the loss function of image generation, the generated output image has the same features as the moving image. Christine et al. [73] converted MRI images into CT ones with CycleGAN, and then used single-mode image similarity measurements for registration.

It can be seen that when GAN is applied to medical image registration, the generator no longer generates images, but it is more like a parameter fitting machine, responsible for fitting registration parameters. The discriminator may serve two purposes: to assess whether a set of parameters is suitable for the target system, or whether or not images processed with this set of parameters are registered.

4.5 Dataset expansion

As a data expansion technology, GAN can generate medical images that are relatively real under visual observation [74]. In this section, the influence of synthetic images on the accuracy of deep learning models is analyzed.

The number of medical images with annotations is usually small. GAN can synthesize images with specific labels to expand datasets. Diaz-Pinto et al. [75] proposed an accurate method for glaucoma assessment based on GAN and

semi-supervised learning. The system is not only able to generate images synthetically but also to automatically provide them with labels. Medical datasets tend to be highly imbalanced due to privacy concerns and non-sharing of data between medical institutions. Salehinejad et al. [76] implemented a DCGAN to create synthetic CXR images based on a medium-sized labeled dataset. A combination of real and synthetic images was used to train deep CNNs to detect the etiology of five types of CXR images. The results show that these networks outperform similar ones trained only with real images. It is doubtful that any synthetic image is suitable for the training process, so efficient selection algorithms for synthetic images are also necessary. Xue et al. [77] proposed a CGAN to generate histopathological images based on classification labels. They also designed a synthetic sample selection algorithm that compares the features of real and synthetic images, where the ground truth label of real images matches the conditional label used to generate synthetic images. Only synthetic images that are close enough to the real-image centroid in the feature space are selected.

5 Semi-supervised learning

5.1 Feature sharing

The classification process starts with extracting appropriate features from the samples, which must show differences among different data categories. Features can form a feature space, where sample points of different categories are separated. Image classification based on deep neural networks mainly uses CNNs to extract features and the last layer to make classification decisions. The whole process is automatically learnt. Although the generator task is generating images and the discriminator task is distinguishing real from fake, their essence is still the CNN structure, with abundant hidden layer features. These can be directly used for classification or to provide auxiliary features for classification. More importantly, both generator and discriminator are trained under unsupervised or semi-supervised conditions, which build the relationship between different image domains. Generators and discriminator features make it possible for semi-supervised or unsupervised learning in other medical image tasks.

The generator usually transforms images between domains or reconstructs images. The generator features need to retain sufficient image structure features. Xie et al. [78] proposed a semi-supervised antagonistic classification model for the classification of benign and malignant pulmonary nodules. The model takes an autoencoder-based unsupervised reconstruction network as generator, and the remaining components include a supervised classification network, a discriminator and a learnable transition layer, which applies generator features to the classification network. Yuan et al. [79] proposed a 3D unified GAN, which unifies the any-to-any modality translation and multimodal segmentation in a single network. Since the anatomical structure is preserved during modality translation, the auxiliary translation task is used to extract modality-invariant features and implicitly generate the additional training data.

The discriminator is used to identify the domain of generated images, so its features retain those of domains. Hu et al. [80] proposed a unified GAN architecture to perform cell-level unsupervised learning. During training, the generator and discriminator learn a distribution that matches that of real data. Then an auxiliary network is used to maximize the mutual information between selected random variables and the generated samples. The weights of the auxiliary network and discriminator heads are shared. Wang et al. [81] proposed a multi-path GAN. The multichannel generator generates a series of sub-fundus images corresponding to scattering diabetic retinopathy features. For input features, each discriminator produces an independent classification result. Results from multiple discriminators are weighted to determine the diabetic retinopathy level, and feature matching between multiple discriminators is implemented.

5.2 Annotations sharing

Deep learning methods are supervised, and image labeling is a difficult task [82]. Because the number of real medical images in training sets is very limited, it is impossible for deep learning models to learn all types of images from them. Aiming at solving the problem of supervised algorithms not performing well with data they have not been exposed to before, GAN can implement semi-supervised learning through annotation sharing. Specifically, annotated datasets can train supervised deep learning models. Annotated images are unified through domain transformation into an annotated image domain, and then supervised deep learning models can be applied to all images in that domain.

Gadermayr et al. [83] used CycleGAN to convert unstained and stained kidney histological images. Based on this, they developed a completely unsupervised segmentation method that relies on image-to-image transformation to obtain color-independent intermediate representations. Chen et al. [84] constructed a cross-modal GAN learning CT and MRI

mapping and an MRI segmentation network, which converted the unlabeled CT images into MRI ones for segmentation. They also proposed a neighborhood-based anchoring method to reduce the ambiguity in cross modal synthesis. In 3D CT scans, organs remain more clearly structured. Zhang et al. [85] proposed a GAN to synthesize 3D CT scan images from X-ray ones, and then used a multi-organ segmentation network for segmentation. Konstantinos et al. [86] proposed a domain adaptive multi-connected adversarial network, where different data types are treated as different domains, making features learnt by segmentation independent of domain-specific factors. Good adaptability was shown with two different brain MRI databases. In [87], also from the point of view of using domains to solve data inconsistent segmentation problems, a network that migrates specific image styles was used. An unannotated color fundus image dataset was changed to annotated dataset style. In this way, the segmentation network trained by annotated datasets can be used to segment unannotated images.

6 Function expansion of GAN

6.1 Extended generator and discriminator

The adversarial learning process of the generator and discriminator produces a large number of advanced semantic features that can be extended to other tasks. The applicability of extended generators and discriminators is not limited, respectively, to image synthesis and to the classification of true and fake images.

Das et al. [88] proposed a generalizable classifier using adversarial learning between generator and discriminator to predict progressive retinal diseases such as age-related macular degeneration and diabetic macular edema. Gu et al. [89] proposed a transfer recurrent feature learning framework for probe-based confocal laser endomicroscopy (pCLE) video classification tasks. In a first phase, the discriminator features of pCLE images are learnt by GAN. In a second phase, discriminator features are applied to a recurrent neural network (RNN) to distinguish between true and false data and lesion grade. It can be seen that the discriminator is mainly expanded into a multiclass classifier.

Some researchers suggested using generators to segment images [87, 90]. In conditional GANs, the generator is usually an ordinary U-net structure, which is completely suitable for segmentation. For example, in tumor segmentation [91] the generator is used to generate segmentation maps, the discriminator has two inputs, namely predicted and real tumor masks, and the loss between masks is used. The work in [92] emphasized adversarial training and proposed an energy based self-encoder as discriminator. Prior knowledge of spine shape is also applied to the network through adversarial learning. Wu et al. [93] proposed an automatic left ventricle segmentation method, which consists of a multi-scale segmentation network and two shared discriminator networks. Two different types of images are alternately applied to the segmentation network to achieve semi-supervised training. Lei et al. [94] suggested using generators to segment skin lesions and designed two discriminators. One of them analyzes the difference between the generated segmentation mask boundary and the ground truth, and the other detects the contextual environment of target objects in the original image.

6.2 Prediction

The prediction task is important in the medical field, because it can provide information about the evolution and estimation of a patient's condition. The time series prediction models commonly used in deep learning include RNN and long short-term memory (LSTM), among others, but these models are more suitable for time series signal vectors, whereas medical images have higher dimensions. GAN provides the possibility of image-level prediction by synthesizing images of nodes in the current time step into images of nodes in the next time step.

Rachmadi et al. [95] proposed a disease evolution predictor (DEP) model to predict the evolution of white matter hyperintensities from baseline to follow-up (i.e., one year later). The DEP model takes a baseline image as input to generate a disease evolution map representing the evolution of the disease. In order to simulate the non-deterministic and unknown parameters involved in the evolution process, a Gaussian noise vector is added to the DEP model as an auxiliary input, which forces the DEP model to simulate a wider range of prediction results. Elazab et al. [96] proposed a stacked 3D GAN for predicting glioma growth. The generator is designed based on a modified 3D U-Net architecture with skip connections to combine hierarchical features. Segmented feature maps are used to guide the generator to generate better images. Wei et al. [97] proposed Sketcher-Refiner GANs to predict demyelination. A first generator generates global anatomical and physiological information. A second one extracts and produces tissue myelin content. Zhao et al. [98] proposed a framework for predicting the progression of Alzheimer's disease, which includes a 3D multi-information GAN

(mi-GAN) and a 3D DenseNet-based multi-class classification network. The generator predicts how a whole brain will look like within a time interval and a classification network determines the clinical stages of the brain.

6.3 Pseudo-healthy synthesis

The task of pseudo-healthy synthesis is to create a healthy image from a sick one. Synthetic healthy images can be used to detect anomalies and understand changes caused by pathology and disease. Tang et al. [99] proposed a deep disentangled generative model (DGM) to generate both abnormal disease residual maps and healthy chest X-ray images from real abnormal chest X-rays images. The DGM consists of three encoder-decoder blocks: the first is used for healthy chest X-rays image synthesis, the second for generating residual maps describing potential lesion areas, and the third for facilitating the training process and enhancing the model's robustness against noise data. Sun et al. [100] proposed an abnormal-to-normal translation GAN (ANT-GAN), which generates healthy medical images based on their abnormal-looking counterparts without the need for paired training data. Xia et al. [101] proposed a model based on cycle-GAN, in which training data used images of healthy domains from different unrelated datasets. A pathological image is firstly disentangled into a corresponding pseudo-healthy image and a pathology segmentation. In the reconstructed network, the pseudo-healthy image is further combined with the segmented image to reconstruct the pathological image. Results for optical coherence tomography in the retina show that this method can correctly identify images containing retinal fluid or highly reflective lesions [102]. The work in [103] adds a simple and efficient constraint to better map abnormal to normal, putting forward stronger requirements for the generator. Domain transformation is usually a change in the overall style of an image, but in this method the generator can only convert the abnormal part. Therefore, it needs to be highly sensitive to the characteristics of abnormal parts.

7 Key challenges and future research directions

7.1 Technology challenges and directions

1) *Evaluation metrics*. The first challenge is the lack of metrics to evaluate the quality of synthetic images. At present, medical image generation has proven to be visually effective, but the quality of generated images still uses traditional evaluation indexes, such as MSE, PSNR, and SSIM, whose mathematical expressions are shown in Table 4. MSE and PSNR just describe the difference between pixels without considering the visual characteristics of human eyes. SSIM only measures the image similarity from brightness, contrast and structure. These evaluation indexes are not objective enough to evaluate the quality of medical image generation [104]. Moreover, it is not necessarily reasonable to evaluate synthetic images by similarity. For example, if the color fundus image of one style is used as the condition to generate the image of another style, it is obvious that the images of these two styles are not similar, which requires more advanced and abstract metrics to measure [105]. Existing works often use physician evaluation to make up the lack of indicators, or the quality of GAN is evaluated by the quality of GAN's downstream tasks.

Loss functions drive networks towards the training process, whereas evaluation indexes check the quality of generated data in the test process, so the two are based on similar ideas. GAN loss functions and evaluation indexes more suitable for medical imaging are also a trend for the future. Unlike other real images, medical ones are often complex in structure, and the details are likely to contain important pathological information. Moreover, there are significant differences between medical images of different types. In GAN's design process, more medical a priori knowledge can

Table 4 Image similarity evaluation indexes

Evaluation index	Expression	Remarks
MSE	$\frac{1}{mn}\sum_{i=0}^{m-1}\sum_{j=0}^{n-1}\left[I(i,j)-K(i,j)\right]^2$	$I(i,j)$ and $K(i,j)$ are pixels in the image
PSNR	$10\cdot\lg\left(\frac{MAX_I^2}{MSE}\right)$	MAX_I^2 is the maximum pixel value in the image
SSIM	$\frac{(2\mu_x\mu_y+C_1)(2\sigma_{xy}+C_2)}{\left(\mu_x^2+\mu_y^2+C_1\right)\left(\sigma_x^2+\sigma_y^2+C_2\right)}$	μ_x and μ_y are mean values of images, σ_x^2 and σ_y^2 are variances of images, C_1 and C_2 are constants, σ_{xy} is covariance

be added, which will be specifically reflected in network structures and loss functions. For example, in [92] the spine is labeled using BtrflyNet with sagittal and coronal information.

2) *Semi-supervised methods*. Traditional supervised methods are useful when training with a large number of labeled data. However, although the learning effect is good, the process of collecting and tagging large datasets is time-consuming, expensive, and error-prone [106]. GAN provides the possibility for weak supervision and non-supervision of medical images. In this paper, the application of GAN semi-supervised learning is considered from two aspects, namely feature sharing and annotation contribution, whose advantages and defects are analyzed.

Feature sharing transfers generator features to deep learning models of unannotated images. As proposed in [79], generators are usually assumed to preserve certain structural features. However, the reserved specific structural features are unprovable and cannot be matched to specific categories. One potential solution is to design feature decoupling modules that define feature structures when generator features are transferred to other tasks.

3) *Domain selection*. In addition to the domain transformation described in Sect. 3.2, many problems can also be abstracted into domain transformation problems, whose pure mathematical description is to map data from one kind of distribution to another, the generator being the mapping between two distributions. Existing works mainly focus on how to do the mapping. Actual medical images are definitely not perfect enough to strictly meet a certain distribution, but it is considered that the same type of data approximately belong to the same distribution. Therefore, there is a lack of attention on the distribution of original data. It is unreasonable to assume that all original data come from the same device or same type means same distribution.

In the authors' opinion introducing domain selection into GAN task is a good solution for this. Domain selection can be implemented in the data preprocessing stage. By calculating distances within the data distribution, the data domain can be determined. It is also feasible to reclassify the data domain by clustering methods. In addition, it is also possible to integrate domain selection into the GAN model. Existing generators are usually self-encoder structures, and the purpose of integrating domain selection into GAN can be achieved by extracting the features of the self-encoder and then performing cluster analysis on them.

4) *Simulation*. GAN's application in medical imaging mainly focuses on laboratory works and has not yet entered the clinical stage. In order to enter it, it is not only necessary to improve a certain technology or a certain index, but also more practical background is required. For example, GAN for surgical simulation is a good combination. Generated images, particularly 3D ones, can not only guide actual surgery but also simulate it. More communication and cooperative research with doctors are needed in this context.

5) *Mode collapse*. GAN is prone to mode collapse in the training process, which leads to strange appearance of generated images, or to the generation of just a certain type of images. The causes of GAN modal collapse are various, including unstable and diminishing gradients, convergence failure, generator dominance etc. Since the basic structure of GAN is the neural network, diminishing gradients may appear in the shallow network during the training, which means that the parameters of the shallow network will be updated slowly and do not match the parameter updating speed of the deep network. For some difficult image synthesis tasks, GAN may not be able to converge. Generator dominance means that the GAN is alternately trained with the generator and discriminator, but there is a possibility that the generator will be dominant. GAN still lacks precise mathematical proof of antagonistic learning and pattern transformation. There is no fundamental solution to mode collapse, and designers can only use more advanced techniques and carefully master the training process. Particularly for medical images, which have high dimensions and complex patterns, pattern collapse is likely to occur.

7.2 Non-technology challenges and directions

1) *Privacy*. The collection of medical images for scientific research requires patient consent. It is not clear if generated images or dataset generated based on them are to be considered as original data or new data, and therefore whether they should be subject to patient consent or not. The legality of new data is also uncertain. Some applications of GAN, such as domain transformation, may even expose more patients' personal privacy than original images. Therefore, for the application of new technology, not only its feasibility but also ethics and law must be considered.

2) *Image confidence*. In the field of medical imaging, the interpretation of an image may affect the life of the patient, so many technologies that are good in other areas for similar purposes may not be applicable in this medical field. Sometimes even a normal medical image will not be given enough trust by doctors, and multi-level detection is still needed. In this context, currently there is no reason for doctors to give trust to images generated by GAN. Cohen et al. [107] questioned the medical images generated by GAN, which may misjudge the medical condition of patients. They trained

a CycleGAN to convert normal brain MRI images to brain MRI images with tumors. In fact, the images generated by their network are visually realistic, but without tumors. There are many reasons behind this. For instance, the generalization performance of a well-trained model is not good, or the transformations between some data domains cannot be accurately carried out. Attention should be paid to this issue, but this does not mean that all GANs will lead to misdiagnosis.

3) *Datasets*. Although there are many publicly available datasets, most of them were created not for use with GAN, but for other medical tasks. The quality of existing medical datasets is spotty, and some are old and scattered. For some tasks, such as the transformation between MRI and CT images, it is difficult to find relevant images of a certain scale. Most researchers collect them by themselves through hospitals.

8 Conclusion

Oriented to GAN for medical imaging, this paper summarizes commonly used GAN methods, medical image synthesis and the function of adversarial learning in other medical image tasks. The relevant papers in the area published in the last five years are reviewed. The challenges of datasets, training methods, reliability, and legality are pointed out. Future directions of unsupervised learning, breakthroughs in clinical needs, and the need for GANs more suitable for medical imaging are also discussed. In general, the existing medical image synthesis technology has a high reliability, and the combination of GAN and other medical image models also produces a good effect. It can be clearly concluded that GAN has great potential and development perspectives in medical imaging. In fact, the whole development trend of artificial intelligence is towards unsupervised (deep) learning.

Authors' contributions Conceptualization, XL, SY, JR; resources: OK, SY, and HL; investigation, XL and YJ; writing—original draft preparation, XL and YJ; writing—review and editing, JR, OK, and YJ; supervision, OK, SY, and HL. All authors read and approved the final manuscript.

Declarations

Competing interests The authors declare no competing interests.

References

1. Krizhevsky A, Sutskever I, Hinton GE. Imagenet classification with deep convolutional neural networks. Adv Neural Inf Process Syst. 2012. https://doi.org/10.1145/3065386.
2. LeCun Y, Bengio Y, Hinton G. Deep learning. Nature. 2015;521(7553):436.
3. Jiang Y, Yin S, Dong J, Kaynak O. A Review on soft sensors for monitoring, control and optimization of industrial processes. IEEE Sens J. 2021;21(11):12868–81.
4. Goodfellow I, Pouget-Abadie J, Mirza M et al. Generative adversarial nets. In: Advances in Neural Information Processing Systems. 2014. p. 2672–80.
5. Creswell A, White T, Dumoulin V, et al. Generative adversarial networks: an overview. IEEE Signal Process Mag. 2018;35(1):53–65.
6. Liu S, Li X, Jiang Y, Luo H, Gao Y, Yin S. Integrated learning approach based on fused segmentation information for skeletal fluorosis diagnosis and severity grading. IEEE Trans Ind Inf. 2021;17(11):7554–63.
7. Yi X, Walia E, Babyn P. Generative adversarial network in medical imaging: a review. Medl Image Anal. 2019;58:
8. Radford A, Metz L, Chintala S. Unsupervised representation learning with deep convolutional generative adversarial networks. In: International conference on image and graphics. 2017. p. 97–108.
9. Ioffe S, Szegedy C. Batch normalization: accelerating deep network training by reducing internal covariate shift. In: International conference on machine learning. 2015. p. 448–56.
10. Glorot X, Bordes A, Bengio Y. Deep sparse rectifier neural networks. In: Proceedings of the fourteenth international conference on artificial intelligence and statistics. 2011. p. 315–23.
11. He K, Zhang X, Ren S, Sun J. Delving deep into rectifiers: surpassing human-level performance on imagenet classification. In: IEEE international conference on computer vision. 2015. p. 1026–34.

12. Mirza M, Osindero S. Conditional generative adversarial nets. Comput Sci 2014;2672–80.
13. Isola P, Zhu J-Y, Zhou T, Efros AA. Image-to-image translation with conditional adversarial networks. In: IEEE conference on computer vision and pattern recognition. 2017. p. 1125–34.
14. Chen X, Duan Y, Houthooft R et al. Infogan: interpretable representation learning by information maximizing generative adversarial nets. In: International conference on neural information processing systems. 2016. p. 2172–80.
15. LeCun Y, Cortes C, Burges ChJC. The MNIST database of handwritten digits. http://yann.lecun.com/exdb/mnist/.
16. Zhu J-Y, Park T, Isola P, Efros AA. Unpaired image-to-image translation using cycle-consistent adversarial networks. In: IEEE international conference on computer vision. 2017. p. 2223–32.
17. Denton EL, Chintala S, Fergus R, et al. Deep generative image models using a laplacian pyramid of adversarial networks. In: International conference on neural information processing systems. 2015. p. 1486–94.
18. Li K, Luo H, Yin S, et al. A novel bias-eliminated subspace identification approach for closed-loop systems. IEEE Trans Ind Electron. 2020;68(6):5197–205.
19. Luo H, Li K, Kaynak O, et al. A robust data-driven fault detection approach for rolling mills with unknown roll eccentricity. IEEE Trans Control Syst Technol. 2019;28(6):2641–8.
20. Bermudez C, Plassard AJ, Davis LT, et al. Learning implicit brain MRI manifolds with deep learning. Int Soc Optics Photon. 2018;10574:105741L.
21. Beers A, Brown J, Chang K et al. High-resolution medical image synthesis usingprogressively grown generative adversarial networks; 2018. arXiv preprint arXiv:1805.03144.
22. BenTaieb A, Hamarneh G. Adversarial stain transfer for histopathology image analysis. IEEE Trans Med Imaging. 2017;37(3):792–802.
23. Wolterink JM, Dinkla AM, Savenije MH, Seevinck PR, van den Berg CA, Sgum Iİ. Deep MR to CT synthesis using unpaired data. In: International workshop on simulation and synthesis in medical imaging. 2017. p. 14–23.
24. Ben-Cohen A, Klang E, Raskin SP, Amitai MM, Greenspan H. Virtual PET images from CT data using deep convolutional networks: initial results. In: International workshop on simulation and synthesis in medical imaging. 2017. p. 49–57.
25. Zhao H, Li H, Maurer-Stroh S, Cheng L. Synthesizing retinal and neuronal images with generative adversarial nets. Med Image Anal. 2018;49:14–26.
26. Wolterink JM, Leiner T, Isgum I. Blood vessel geometry synthesis using generative adversarial networks; 2018. arXiv preprint arXiv:1804.04381.
27. Han C, Hayashi H, Rundo L et al. GAN-based synthetic brain MR image generation. International symposium on biomedical imaging. 2018. p. 734–8.
28. Calimeri F, Marzullo A, Stamile C, Terracina G. Biomedical data augmentation using generative adversarial neural networks. In: International conference on artificial neural networks. Springer; 2017. pp. 626–634.
29. Salehinejad H, Valaee S, Dowdell T, Colak E, Barfett J. Generalization of deep neural networks for chest pathology classification in x-rays using generative adversarial networks. In: 2018 IEEE international conference on acoustics, speech and signal processing (ICASSP). IEEE; 2018. pp. 990–994, IEEE.
30. Kitchen A, Seah J. Deep generative adversarial neural networks for realistic prostate lesion mri synthesis; 2017. arXiv preprint arXiv:1708.00129.
31. Chuquicusma MJ, Hussein S, Burt J, Bagci U. How to fool radiologists with generative adversarial networks? A visual Turing test for lung cancer diagnosis. In: 2018 IEEE 15th International Symposium on Biomedical Imaging (ISBI 2018). IEEE; 2018. pp. 240–244.
32. Baur C, Albarqouni S, Navab N. Melanogans: high resolution skin lesion synthesis with gans; 2018. arXiv preprint arXiv:1804.04338.
33. Baur C, Albarqouni S, Navab N. Generating highly realistic images of skin lesions with GANs. OR 2.0 context-aware operating theaters, computer assisted robotic endoscopy, clinical image-based procedures, and skin image analysis. Cham: Springer; 2018. p. 260–267.
34. Yi X, Walia E, Babyn P. Unsupervised and semi-supervised learning with categorical generative adversarial networks assisted by wasserstein distance for dermoscopy image classification; 2019. arXiv preprint arXiv:1804.03700.
35. Frid-Adar M, Diamant I, Klang E, et al. Gan-based synthetic medical image augmentation for increased CNN performance in liver lesion classification. Neurocomputing. 2018;321:321–31.
36. Nie D, Trullo R, Lian J, et al. Medical image synthesis with context-aware generative adversarial networks. In: International conference on medical image computing and computer-assisted intervention. Springer; 2017. pp. 417–425.
37. Zhao M, Wang L, Chen J et al. Craniomaxillofacial bony structures segmentation from MRI with deep-supervision adversarial learning. In: International conference on medical image computing and computer assisted intervention. Springer, 2018. pp. 720–727.
38. Zhang Z, Yang L, Zheng Y. Translating and segmenting multimodal medical volumes with cycle-and shape-consistency generative adversarial network. In: Proceedings of the IEEE conference on computer vision and pattern recognition; 2018. pp. 9242–9251.
39. Chartsias A, Joyce T, Dharmakumar R, Tsaftaris SA. Adversarial image synthesis for unpaired multi-modal cardiac data. In: International workshop on simulation and synthesis in medical imaging. Springer; 2017. pp. 3–13.
40. Hiasa Y, Otake Y, Takao M, Matsuoka T, Takashima K, Carass A, Prince JL, Sugano N, Sato Y. Cross-modality image synthesis from unpaired data using cyclegan. In: International workshop on simulation and synthesis in medical imaging. Springer; 2018. pp. 31–41.
41. Bi L, Kim J, Kumar A, Feng D, Fulham M. Synthesis of positron emission tomography (PET) images via multi-channel generative adversarial networks (GANs). In: Molecular imaging, reconstruction and analysis of moving body organs, and stroke imaging and treatment. Springer; 2017. pp. 43–51.
42. Wei W, Poirion E, Bodini E et al. Learning myelin content in multiple sclerosis from multimodal MRI through adversarial training. In: International conference on medical image computing and computer-assisted intervention. Springer; 2018. pp. 514–522.
43. Armanious K, Yang C, Fischer M et al. Medgan: medical image translation using gans; 2018. arXiv preprint arXiv:1806.06397.
44. Ben-Cohen A, Klang E, Raskin SP, et al. Cross-modality synthesis from CT to PET using FCN and GAN networks for improved automated lesion detection. Eng Appl Artif Intell. 2019;78:186–94.
45. Zanjani FG, Zinger S, Bejnordi BE, van der Laak JA, et al. Histopathology stain-color normalization using deep generative models. In: International conference on medical imaging with deep learning. 2018.

46. Bayramoglu N, Kaakinen M, Eklund L, Heikkila J. Towards virtual H&E staining of hyperspectral lung histology images using conditional generative adversarial networks. In: Proceedings of the IEEE international conference on computer vision; 2017. pp. 64–71.
47. Costa P, Galdran A, Meyer MI, et al. End-to-end adversarial retinal image synthesis. IEEE Trans Med Imaging. 2017;37(3):781–91.
48. Guibas JT, Virdi TS, Li PS. Synthetic medical images from dual generative adversarial networks; 2017. arXiv preprint arXiv:1709.01872.
49. Hu Y, Gibson E, Lee L-L et al. Freehand ultrasound image simulation with spatially conditioned generative adversarial networks. In: Molecular imaging, reconstruction and analysis of moving body organs, and stroke imaging and treatment. Springer; 2017. pp. 105–115.
50. Tom F, Sheet D. Simulating patho-realistic ultrasound images using deep generative networks with adversarial learning. In: 2018 IEEE 15th international symposium on biomedical imaging (ISBI 2018). IEEE; 2018. pp. 1174–1177.
51. Mahapatra D, Bozorgtabar B, Thiran J-P, Reyes M. Efficient active learning for image classification and segmentation using a sample selection and conditional generative adversarial network. In: International conference on medical image computing and computer-assisted intervention. Springer; 2018. pp. 580–588.
52. Olut S, Sahin YH, Demir U, Unal G. Generative adversarial training for MRA image synthesis using multi-contrast MRI. In: International workshop on predictive intelligence in medicine. Springer; 2018. pp. 147–154.
53. Almalioglu Y, Ozyoruk KB, Gokce A, et al. EndoL2H: deep super-resolution for capsule endoscopy. IEEE Trans Med Imaging. 2020; (99):1–1.
54. Ma J, Cheng S, Yu J, et al. PathSRGAN: multi-supervised super-resolution for cytopathological images using generative adversarial network. IEEE Trans Med Imaging. 2020; (99):1–1.
55. Ronneberger O, Fischer P, Brox T. U-net: convolutional networks for biomedical image segmentation. International conference on medical image computing and computer-assisted intervention. Cham: Springer; 2015. Pp. 234–241.
56. Ravì D, Szczotka AB, Pereira SP, Vercauteren T. Adversarial training with cycle consistency for unsupervised super-resolution in endomicroscopy. Med Image Anal. 2019;53:123–31.
57. You C, Li G, Zhang Y, et al. CT super-resolution GAN constrained by the identical, residual, and cycle learning ensemble (GAN-CIRCLE). IEEE Trans Med Imaging. 2019;39(1):188–203.
58. Das V, Dandapat S, Bora PK. Unsupervised super-resolution of OCT images using generative adversarial network for improved age-related macular degeneration diagnosis. IEEE Sens J. 2020; (99):1–1.
59. Li Z, Wang Y, Yu J. Reconstruction of thin-slice medical images using generative adversarial network. In: International workshop on machine learning in medical imaging. Springer; 2017. pp. 325–333.
60. Chen Y, Shi F, Christodoulou AG et al. Efficient and accurate MRI super-resolution using a generative adversarial network and 3D multi-level densely connected network. In: International conference on medical image computing and computer-assisted intervention. Springer; 2018. pp. 91–99.
61. Sánchez I, Vilaplana V. Brain MRI super-resolution using 3D generative adversarial networks. International conference on medical imaging with deep learning. 2018.
62. Yang Q, et al. Low-dose CT image denoising using a generative adversarial network with Wasserstein distance and perceptual Loss. IEEE Trans Med Imaging. 2018;37(6):1348–57.
63. Wolterink JM, et al. Generative adversarial networks for noise reduction in low-dose CT. IEEE Trans Med Imaging. 2017;36(12):2536–45.
64. Choi K, Lim JS, Kim S. StatNet: statistical image restoration for low-dose CT using deep learning. IEEE J Sel Topics Signal Process. 2020;99:1–1.
65. Zhou Z, et al. Image quality improvement of hand-held ultrasound devices with a two-stage generative adversarial network. IEEE Trans Biomed Eng. 2019;67(1):298–311.
66. Chen L, et al. De-smokeGCN: generative cooperative networks for joint surgical smoke detection and removal. IEEE Trans Med Imaging. 2019;39(5):1615–25.
67. Yang G, Yu S, Dong H, et al. Dagan: deep de-aliasing generative adversarial networks for fast compressed sensing mri reconstruction. IEEE Trans Med Imaging. 2017;37(6):1310–21.
68. Seitzer M, Yang G, Schlemper J et al. Adversarial and perceptual refinement for compressed sensing MRI reconstruction. In: International conference on medical image computing and computer-assisted intervention. Springer; 2018. pp. 232–240.
69. Quan TM, Nguyen-Duc T, Jeong WK. Compressed sensing MRI reconstruction with cyclic loss in generative adversarial networks. IEEE Trans Med Imaging. 2017; 99.
70. Hu Y, Gibson E, Ghavami N et al. Adversarial deformation regularization for training image registration neural networks. In: International conference on medical image computing and computer assisted intervention. Springer; 2018. pp. 774–782.
71. Yan P, Xu S, Rastinehad AR, Wood BJ. Adversarial image registration with application for MR and TRUS image fusion. In: International workshop on machine learning in medical imaging. Springer; 2018. pp. 197–204.
72. Mahapatra D, Antony B, Sedai S, Garnavi R. Deformable medical image registration using generative adversarial networks. In: 2018 IEEE 15th international symposium on biomedical imaging (ISBI 2018). IEEE; 2018. pp. 1449–1453.
73. Tanner C, Ozdemir F, Profanter R et al. Generative adversarial networks for MR-CT deformable image registration; 2018. arXiv preprint arXiv:1807.07349.
74. Jiang Y, Yin S, Kaynak O. Data-driven monitoring and safety control of industrial cyber-physical systems: basics and beyond. IEEE Access. 2018;6:47374–84.
75. Diaz-Pinto A, et al. Retinal image synthesis and semi-supervised learning for glaucoma assessment. IEEE Trans Med Imaging. 2019;38(9):2211–8.
76. Salehinejad H, Colak E, Dowdell T, et al. Synthesizing chest X-ray pathology for training deep convolutional neural networks. IEEE Trans Med Imaging. 2019;38(5):1197–206.
77. Xue Y, et al. Selective synthetic augmentation with HistoGAN for improved histopathology image classification. Med Image Anal. 2021;67: 101816.
78. Yutong X, et al. Semi-supervised adversarial model for benign–malignant lung nodule classification on chest CT. Med Image Anal. 2019;57:237–48.

79. Wenguang Yuan A, et al. Unified generative adversarial networks for multimodal segmentation from unpaired 3D medical images. Med Image Anal. 2020;64:101731.
80. Bo H, et al. Unsupervised learning for cell-level visual representation in histopathology images with generative adversarial networks. IEEE J Biomed Health Inf. 2017;23(3):1316–28.
81. Wang S, et al. Diabetic retinopathy diagnosis using multichannel generative adversarial network with semisupervision. IEEE Trans Autom Sci Eng. 2020;99:1–12.
82. Li X, Jiang Y, Yin S. Lightweight attention convolutional neural network for retinal vessel image segmentation. IEEE Trans Ind Inf. 2020;17(3):1958–67.
83. Gadermayr M, et al. Generative adversarial networks for facilitating stain-independent supervised and unsupervised segmentation: a study on kidney histology. IEEE Trans Med Imaging. 2019;38(10):2293–302.
84. Chen X, et al. One-shot generative adversarial learning for MRI segmentation of craniomaxillofacial bony structures. IEEE Trans Med Imaging. 2019;99:1–1.
85. Zhang Y, et al. Unsupervised X-ray image segmentation with task driven generative adversarial networks. Med Image Anal. 2020. https://doi.org/10.1016/j.media.2020.101664.
86. Zhao H, Li H, Maurer-Stroh S, et al. Supervised segmentation of un-annotated retinal fundus images by synthesis. IEEE Trans Med Imaging. 2019;38(1):46–56.
87. Huo Y, Xu Z, Bao S et al. Splenomegaly segmentation using global convolutional kernels and conditional generative adversarial networks. Medical Imaging. 2018: Image Processing, vol. 10574, p. 1057409, International Society for Optics and Photonics, 2018.
88. Das V, Dandapat S, Bora PK. A data-efficient approach for automated classification of OCT images using generative adversarial network. IEEE Sens Lett. 2020;4(1):1–4.
89. Gu Y, Vyas K, Yang J, Yang G-Z. Transfer recurrent feature learning for endomicroscopy image recognition. IEEE Trans Med Imaging. 2019;38(3):791–801.
90. Son J, Park SJ, Jung K-H. Retinal vessel segmentation in fundoscopic images with generative adversarial networks; 2017. arXiv preprint arXiv:1706.09318.
91. Xue Y, Xu T, Zhang H, Long LR, Huang X. Segan: adversarial network with multi-scale l 1 loss for medical image segmentation. Neuroinformatics. 2018;16(3–4):383–92.
92. Sekuboyina A, Rempfler M, Kukačka et al. Btrfly net: vertebrae labelling with energy-based adversarial learning of local spine prior. In: International conference on medical image computing and computer-assisted intervention. Springer; 2018. p. 649–657.
93. Wu H, et al. Automated left ventricular segmentation from cardiac magnetic resonance images via adversarial learning with multi-stage pose estimation network and co-discriminator. Med Image Anal. 2021;68:101891.
94. Lei B, et al. Skin lesion segmentation via generative adversarial networks with dual discriminators. Med Image Anal. 2020;64: 101716.
95. Rachmadi MF, et al. Automatic spatial estimation of white matter hyperintensities evolution in brain MRI using disease evolution predictor deep neural networks. Med Image Anal. 2020;63:101712.
96. Elazab A, et al. GP-GAN: Brain tumor growth prediction using stacked 3D generative adversarial networks from longitudinal MR Images. Neural Netw. 2020;132:321–32.
97. Wei W, et al. Predicting PET-derived demyelination from multimodal MRI using sketcher-refiner adversarial training for multiple sclerosis. Med Image Anal. 2019;58: 101546.
98. Zhao Y, et al. Prediction of Alzheimer's disease progression with multi-information generative adversarial network. IEEE J Biomed Health Inf. 2020;25(3):711–9.
99. Tang Y, et al. A disentangled generative model for disease decomposition in chest X-rays via normal image synthesis. Med Image Anal. 2020;67: 101839.
100. Sun L, et al. An adversarial learning approach to medical image synthesis for lesion detection. IEEE J Biomed Health Inf. 2020;24(8):2303–14.
101. Xia T, Chartsias A, Tsaftaris SA. Pseudo-healthy synthesis with pathology disentanglement and adversarial learning. Med Image Anal. 2020;64: 101719.
102. Schlegl T, Seeböck P, Waldstein SM, Schmidt-Erfurth U, Langs G. Unsupervised anomaly detection with generative adversarial networks to guide marker discovery. In: International conference on information processing in medical imaging. Springer; 2017. pp. 146–157.
103. Chen X, Konukoglu E. Unsupervised detection of lesions in brain MRI using constrained adversarial auto-encoders; 2018. arXiv preprint arXiv:1806.04972.
104. Randulfe JL et al. A quantitative method for selecting denoising filters, based on a new edge-sensitive metric. In: Proceedings of 2017 IEEE International Conference on Industrial Technology, ICIT2017, pp. 974–979
105. Yin S, Rodriguez J, Jiang Y. Real-time monitoring and control of industrial cyberphysical systems with integrated plant-wide monitoring and control framework. IEEE Ind Electron Mag. 2019;13(4):38–47.
106. Jiang Y, Yin S, Li K, Luo H, Kaynak O. Industrial applications of digital twins. Phil Trans R Soc A. 2021;379:20200360.
107. Cohen JP, Luck M, Honari S. Distribution matching losses can hallucinate features in medical image translation. arXiv preprint arXiv:1805.08841.